The University of Strathclyde

Department of Physics

Temperature and stress measurements based on praseodymium (Pr^{3+}) doped optical fibre

by

Yuanyuan Wei

A thesis presented in fulfilment of the requirements for the degree of Master of Philosophy in Physics

2013

This thesis is the result of the author's original research. It has been composed by the author and has not been previously submitted for examination which has led to the award of a degree.

Signed: Date:

Acknowledgements

I would like to thank Dr Thomas Han and Dr Ivan Ruddock as my supervisors in my postgraduate study. Their advices and guidance give me a lot of help.

I would also like to thank my friends. They inspire me and give me some advices, especially providing me a place to live when I could not rent a house for short term.

At last, I would like to thank my parents. They give me this chance to study overseas and support me anytime.

Abstract

In this thesis, praseodymium (Pr^{3+}) doped optical fibre is investigated as a physical sensor measuring temperature and stress.

The project investigates the spectroscopic properties of Pr^{3+} doped silica fibre as a potential sensor for environmental properties such as temperature and stress. The measurements have two parts: spectral and decay time. In the spectral part, Pr^{3+} doped optical fibre is excited by an OPO laser or a continuous-wave Argon-ion laser. The intensity and wavelength of the fluorescence are used to determine the effect of temperature and stress. In the decay time measurements, the fibre is excited by the OPO laser. These measurements revealed a 2 components decay – a fast component in the order of $5\mu s$ and a slower component in the order of $300\mu s$.

Within the experimental constraints on the range on temperature and stress of 0-100℃ and 0-900g respectively, the wavelengths of the three emission peaks and the excitation peak do not show any obvious change and the FWHM of the three emission peaks also does not show any trends or changes.

Only two of the three emission peaks were measured in the decay time measurements. The decay time is measured in the temperature range 20-100℃, the stretch range 0-450g and compression range 0-5kg. Two components of the decay time for the two emission peaks are detected in the experiments. The fast component of the decay time of both emission peaks with temperature shows quite little decrease. The slow component of the decay time of the two emission peaks shows a positive trend with weight. These results follow similar trend for other rare earth doped optical fibre [1].

Contents

1 Introduction

Sensors are used in everyday and everywhere, even though they are not obvious in our daily life. A sensor can measure a physical quantity and produce an output signal that can be measured. Sensor should be sensitive to the targeted property only and should not influence it or affected by other external factors.

Sensors can be classified into three types: physical, chemical and biological. Physical sensors are usually based on the measurements of parameters such as temperature, force, heat, light, electricity, magnetism, sound and other physical properties. Chemical sensors based on chemical reaction, and biological sensors use enzyme, antibody and hormone

Temperature and stress measurements are required in many fields of today's work. Due to the special advantages of optical fibre sensors, optical fibre sensors are considered for the measurements of temperature and stress.

There are some optical fibre sensing technologies used to measure temperature and stress such as distributed optical fibre sensor, interferometric optical fibre sensor and fluorescence optical fibre senor [2].

Rare earth doped optical fibre are usually used in the fluorescence optical fibre sensor. This project aim is to invest how the fluorescence properties influenced by temperature and stress in Pr^{3+} doped optical fibre.

In chapter 2, non-optical measurements systems and optical measurements are introduced with the work principle, advantages and disadvantages respectively. Compare to them, optical fibre sensors have some special advantages, but they also

have some disadvantages. The measurements of temperature and stress are based on the properties of fluorescence. The description of fluorescence and some fluorescence applications are also introduced.

Pr^{3+} doped optical fibre was chosen for this investigation. Chapter 3 will give some information about the silica optical fibre and rare earth elements. The manufacture of the Pr^{3+} doped optical fibre is also introduced in this chapter.

Chapter 4 describes temperature and stress effects on fluorescence. It mainly talks about how temperature or stress influence the decay time. In this chapter, it also introduced the devices used in the experiments and the experiment arrangement of temperature and stress measurements. Both OPO laser and cw-Argon laser are used in the frequency part. Only the OPO laser is used in the decay time part. The temperature change is achieved by using a water bath. A pulley block is used to stretch fibre to get the stress change. But in the decay time part, two wooden blocks with smooth formica surface are also used to compress the fibre.

Results of the measurements are shown in chapter 5. The experiments are based on the spectroscopy of fluorescence, it includes intensity, wavelength and decay time of fluorescence. The experiments are divided into two parts: spectral and decay time. In the spectral part, it mainly focused on the intensity and wavelength of fluorescence. In the decay time part, it measured the decay time of fluorescence. In the spectral part, the wavelengths of the three emission peaks (labelled as A, B and C) are measured. In the decay time part, only peak A and C are measured because the intensity of peak B is too low. Two components of decay time are detected in the measurements.

At last, the results are compared to other rare earth doped optical fibre and Koziol's

work and discuss the reason of the differences. Meanwhile, some advices are given for the future work in chapter 6.

2 Background and basic theory

2.1 Introduction

There are many sensors used in the measurement of temperature and stress. They could be divided into two groups: non-optical and optical. The difference between them is whether the measuring systems use optical techniques or not. Different environment requires different types of measurement systems.

Thermometer is the simplest device used to measure temperature. And spring dynamometer is the simplest device to measure force. They could work in the normal environment and deal with common cases. With the development of technology, many new conditions of measurement need to be satisfied in modern environment. For example, devices need to work in harsh environments, high voltage or toxic environment and in extreme temperature situations. In all cases, measurement range, accuracy, resolution and repeatability of the sensor are all essential to their specific applications.

2.1.1 Absorption

If a normally transparent material is doped with some impurity ions which has energy levels in the materials transparent region one can easily measure, these energy levels using the optical absorption technique. These energy levels of the impurity ions are sensitive to the ions' local environment. Hence temperature or stress experienced by the material can be determined indirectly.

The absorption temperature measurement system has simple optical arrangement and linear response. However, its measure range is limited by the semiconductor material and the measurement system is hard to bond to optical fibres [3].

2.1.2 Fluorescence

Fluorescence has three properties that can be used to measure temperature and stress: wavelength shift, fluorescence intensity ratio and fluorescence decay time. Due to the thermal expansion, temperature changes the structure of the lattice in the optical fibre. Stress has the same influence. The change of the lattice structure can cause the shift of wavelength.

Fluorescence intensity ratio uses two relate energy levels that are closely separated. Due to Boltzmann distribution, the populations of the two related energy levels change with temperature. The fluorescence intensity is related the population of the energy level, so the fluorescence intensity ratio could be used to measure temperature,

$$\text{FIR} = \frac{N_2}{N_1} = \frac{I_{2j}}{I_{2j}} = \frac{g_2\sigma_{2j}\omega_{2j}}{g_1\sigma_{1j}\omega_{1j}} exp\left[\frac{-\Delta E}{kT}\right]$$

where N_i is the number of ions, I_{ij} is the fluorescence intensity, g_i is the degeneracy, σ_{ij} is the emission cross section, ω_{ij} is the angular frequency of fluorescence transitions from the thermalizing energy level to a terminal level. ΔE is the energy difference between the two thermally linked levels. k is the Boltzmann constant and *T* is the absolute temperature [4].

Fluorescence intensity ratio is strain-independent, and it has wide measure range and

good accuracy. In the low temperature area, fluorescence intensity ratio is not sensitive. The price of the measurement system is quite high [4].

Fluorescence decay time is the average time of ions stay in the excite state. The intensity of the fluorescence is decay exponentially with time after excitation ceased. The decay time is defined as the time when the intensity of fluorescence decreases to $\frac{1}{e}$ of its original intensity. It can be described as:

$$\mathrm{I}(t) = I_0 exp - (t/\tau)$$

where I_0 is the original intensity and τ is the decay time [1].

Fluorescence decay time has simple arrangement and it has wide measure range. The problem with the decay time measurement system is that it is affected by temperature and stress at the same time [1].

Due to the intensity of fluorescence could be affected by many factors like coupling and scattering, the temperature or stress measurement based on the intensity of fluorescence could not reach high accuracy. Whereas measurement based on the decay time of fluorescence is immune to these factors and potentially can achieved high accuracy and sensitivity [2].

2.2 Optical fibre sensors

Sensors have many types. Fibre-optic sensing is a new kind of sensor which is based on optical fibre. Photonic sensor first appeared in the mid 1967s [5]. It used bifurcated fibre bundles. Half of the fibre is used to illuminate a surface and the other

half received the reflected light from the surface. Through this process, it can determine the distance between the fibre end and surface.

The main part of the fibre-optic sensing is the optical fibre. Depending on the way of the optical fibre is used, it can be divided into two groups: active and passive. In the latter case, the fibre is a passive element acting only as a light guide. In the active case, the fibre itself is the sensing element and light guide as well.

Fibre-optic sensing has its special advantages. It has small size and simple structure and immune to electromagnetic interference. Due to optical fibre material, it can work in high voltage, high ionising radiation and harsh chemical environment.

Fibre-optic sensing also has its disadvantages. Active sensors need special optical fibre which is expensive, and special test devices are needed in the fibre-optic sensing.

2.3 Fluorescence

When light illuminates on atoms, electrons around the atomic nucleus will be excited to high energy level. Due to high energy levels are unstable, electrons will return to the ground state. In the process, energy is released in the form of light fluorescence or transmits to other electrons. The excitation and emission process can be described by two equations,

$$\text{Excitation: } S_0 + hv_{ex} \rightarrow S_1$$

$$\text{Emission: } S_1 \rightarrow S_0 + hv_{em} + heat$$

where h is the Planck's constant and the ν is the frequency of the light, S_0 is the ground state and S_1 is the excited state of fluorescent molecule. The whole process could be clearly described in a Jablonski energy diagram.

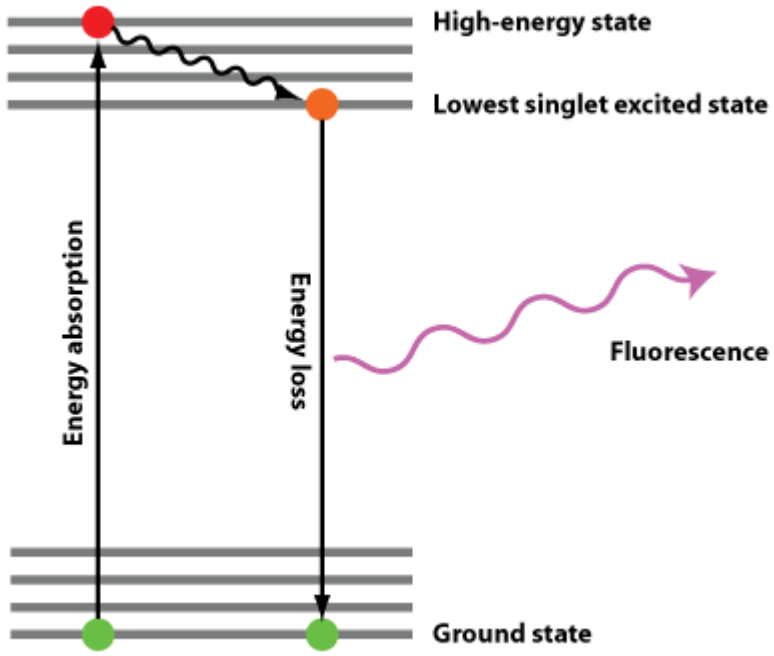

Figure 2.5 [6]: This is the Jablonski energy diagram. Electrons in the ground state transit to high energy level after absorbing energy. The non-radiative transition occurs when the electrons transit from the high energy level to the lowest excited state. Fluorescence is produced in the transition from excited states to low energy state.

In most cases, the emission wavelength is usually longer than the absorbed wavelength. Two-photon absorption may occur when either the absorption strength or excitation energy is large. This phenomenon leads to the emission wavelength shorter than the absorbed wavelength. If the emission wavelength is the same as the absorbed wavelength, it is called resonance fluorescence.

Fluorescence has many applications in modern day living. The fluorescent lamp which is based on fluorescence is the most common application in daily lives. The traditional fluorescent lamp uses excited mercury atoms emitting in the ultraviolet. The ultraviolet rays in turns excite the rare earth ions that are deposited as a coating on the inside surface of the glass envelope of the lamp, the rare earth ions in turn emit in the visible region. A combination of different wavelengths gives the sensation of white light output.

Fluorescence techniques have been widely used in chemical, biological and medical fields. For example, fluorescence is used to detect and analysis the structure of deoxyribonucleic acid (DNA) and protein. Ethidium bromide organism is a kind of fluorescent dye which is used to dye the DNA. It only can emit very weak fluorescence in the solution. However, when it is embedded between the base pairs of double-stranded nucleic acid and combines with the DNA molecule, its fluorescence intensity is much larger than it in the free solution [7].

Florescence microscopy imaging technique is another important application. For example, when the red blood cells contain lead elements or lack of iron elements, they will produce zinc protoporphyrin to replace the normal protoheme. Zinc protoporphyrin has high fluorescence strength, this property can be used in the dianoetic of pathogenesis [8].

3 Rare earth doped fibre

3.1 Silica-based optical fibre

Optical fibre usually made from silica, but there are some special fibre made from fluoride, phosphates and chalcogenides. Plastic optical fibre is a new kind of optical fibre that can be produced simply, cheaply and has low weight.

Silica optical fibre has excellent optical transmission characteristics, it has low loss only about 1 db/km and wide bandwidth. The lowest loss is 0.2db/km at 1.55μm [9]. Silica optical fibre could work in complex environment. It can withstand high temperature and has high mechanical strength. This means that it could be pulled and bent within a certain range.

Silicon fibre has been used widely in optical telecommunications. It mainly depends on total internal reflection. Total internal reflection is the phenomenon when light travels from a high refractive index medium to a low refractive index medium at angles larger than a the critical angle, all the light reflect and confined within the high refractive index medium. The core of optical fibre usually doped with other materials to raise the refractive index. The commonly used materials are Germanium dioxide and Aluminium oxide.

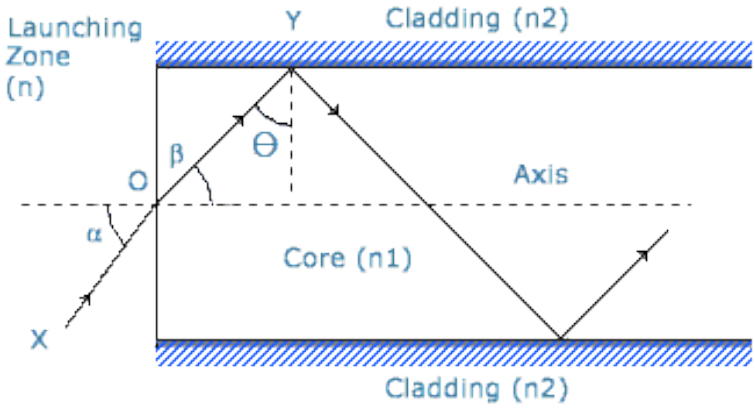

Figure 3.1 [10]: Total internal reflection occurs at the boundary of the core and cladding for a step-change refractive index type fibre.

Optical fibre usually has three parts: core, cladding and buffer. Cladding has lower refractive index than the core. Buffer is designed to protect the fibre from physical damage.

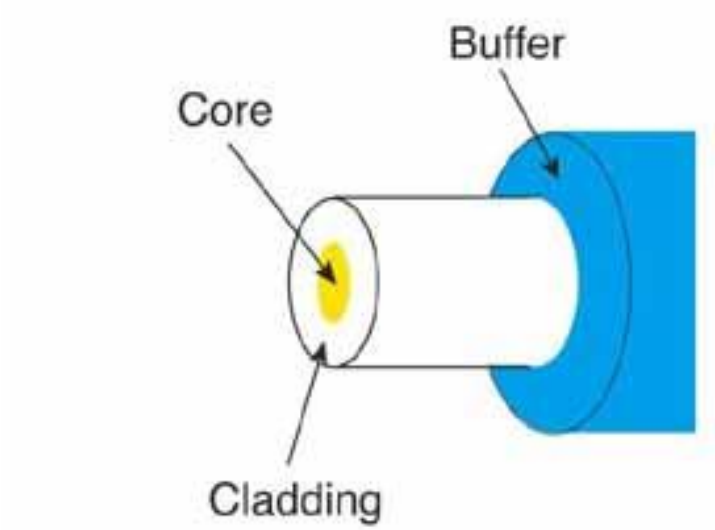

Figure 3.2 [11]: Optical fibre usually includes core, cladding and buffer.

Optical fibre could be largely divided into two groups: single mode and multimode. In common case, single mode fibre‘s core diameter is about 8-10μm while multiple mode is greater than 50μm or 62.5 μm [12]. Fibre also can be divided into

step-index and graded-index.

Due to the radius of the core is very small, single mode fibres only transit the fundamental mode light. The radius of the core of multimode fibre is much larger, so it could transit higher order modes light. Lights have the same transit velocity in the fibre, but different mode lights have different paths. Hence the time needed to reach the detector is different. The time difference will cause pulse boarding which is related to the transit distance. In this case, single mode fibre should be used for remote transition [13].

3.2 Rare earth elements

Rare earth group has 17 elements. Rare earth elements co-exist in the nature and share similar properties.

Although rare earth elements have similar properties, there are still small differences between them. These differences are determined by the structure and radius of their atoms and ions. Based on the lowest energy principle (electrons prefer to low energy atomic orbital), lanthanide atoms have two ground state electron configurations: $[\mathrm{Xe}]4f^n6s^2$ or $[\mathrm{Xe}]4f^{n-1}5d^16s^2$. When the atom is excited by an electromagnetic radiation or heat, they lose either the $4f^16s^2$ or the $5d^16s^2$. Figure 3.3 shows the outside electron structure of the rare earth elements.

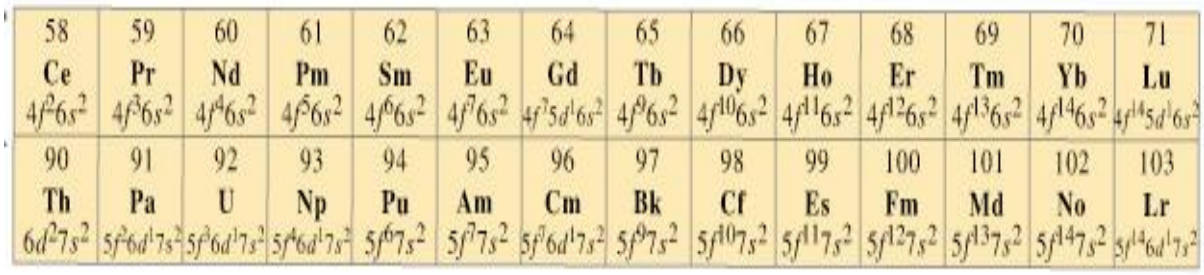

Figure 3.3 [14]: This diagram shows the rare earth elements position in the periodic table and their outside electron structure.

With the atomic number increase, the number of electrons also increases. The increased electrons enter the 4f subshell, and the structure of outer subshells does not change. Due to the radial distribution of 4f subshell could not totally shield the attraction between the nuclear charge and the outer electrons, the attraction increase with the nuclear charge increase. In this case, the radius of lanthanide atoms and the positive trivalent ions decrease with the atomic number increase. This is the Lanthanide contraction.

For lanthanide ions, there are still the $5s^2 5p^6$ electron shell outsides the 4f. Due to the shielding effect by these two full electron shells, the 4f electrons experienced lesser effect from their surrounding elements in the compound. Therefore, the absorption and emission spectra of lanthanide compounds and free ions have similar narrow line structure.

4f subshell has 7 orbitals, electrons progressively filling these orbitals. For rare earth ions, the electrons distribution could produce many energy levels and spectroscopic terms. Figure 3.4 is the Dieke energy diagram which shows the energy levels of the rare earth trivalent ions.

Some excited states of rare earth ions have longer decay time. For rare earth ions, the

4f-4f transition is forbidden because of the Laporte selection rule [15]. The probability is quite low, hence the decay time of the excited states is relatively long in the order of tens of μs.

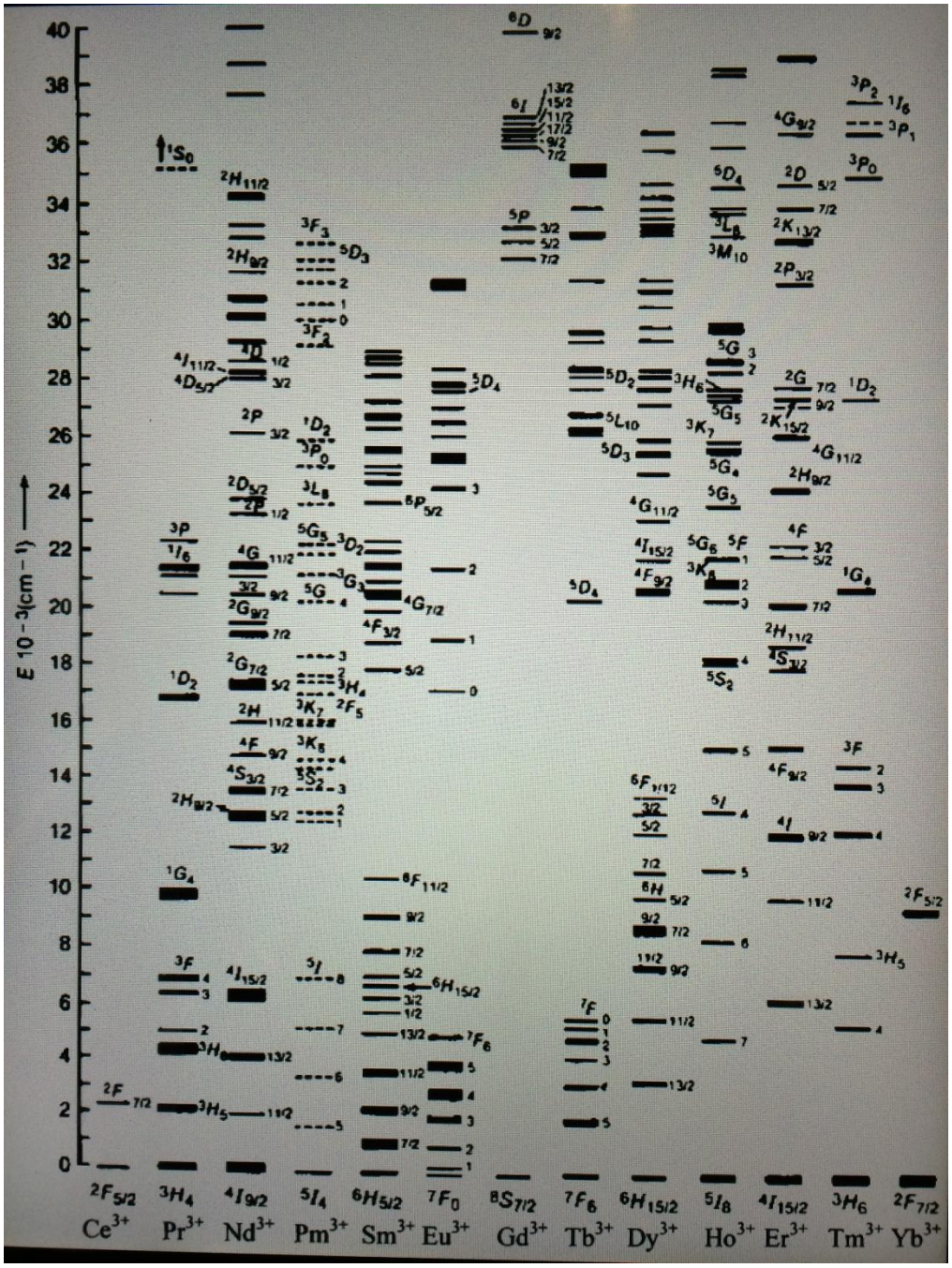

Figure 3.4 [16]: This is the Dieke energy diagram, it shows the trivalent rare-earth ions energy levels.

3.3 Praseodymium. Pr

Praseodymium, Pr, was discovered in 1885 by C.F.Aver von Welesbach [17]. At first, Swedish chemist Carl Gustav Mosander discovered didymium which is a rare earth oxide. After few years, Welesbach was able to separate the didymium into two different elements, praseodymium and neodymium. Praseodymium has six electron shells, electrons distribute as 2,8,18,21,8,2 which is shown in figure 3.5. Its inner electrons configuration is same as Xe which is $4f^3 6s^2$. Praseodymium's crystal structure is hexagonal. Praseodymium usually ionized to Pr^{3+} with the loss of three electrons $4f^1 6s^2$.

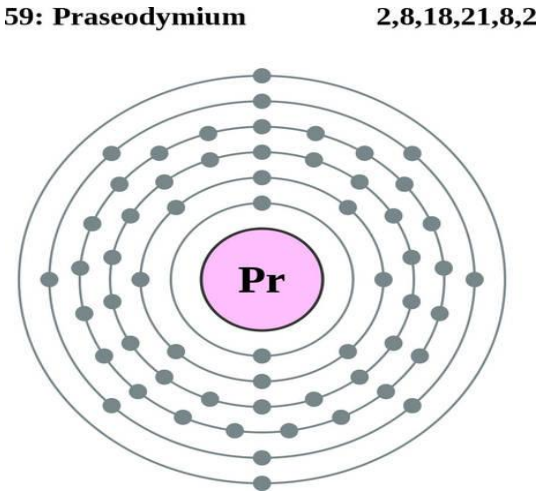

Figure 3.5 [18]: Praseodymium electrons structure

3.4 Praseodymium doped fibre

Praseodymium doped fibre is made by modified chemical vapour deposition (MCVD). It usually use $SiCl_4$ and $GeCl_4$ vapor. In the heating conditions, they will react with oxygen and produce SiO_2 ,GeO_2 and Cl_2 [19]. Based on thermophoresis,

they will deposit on the inside surface of the tube. Then the Praseodymium vapour is introduced and deposit a second layer on the inside surface of the tube. At last, the tube collapses into a preform by increasing the temperature of heating. The fibre is then drawn out from the preform. Figure 3.6 illustrates part of the process.

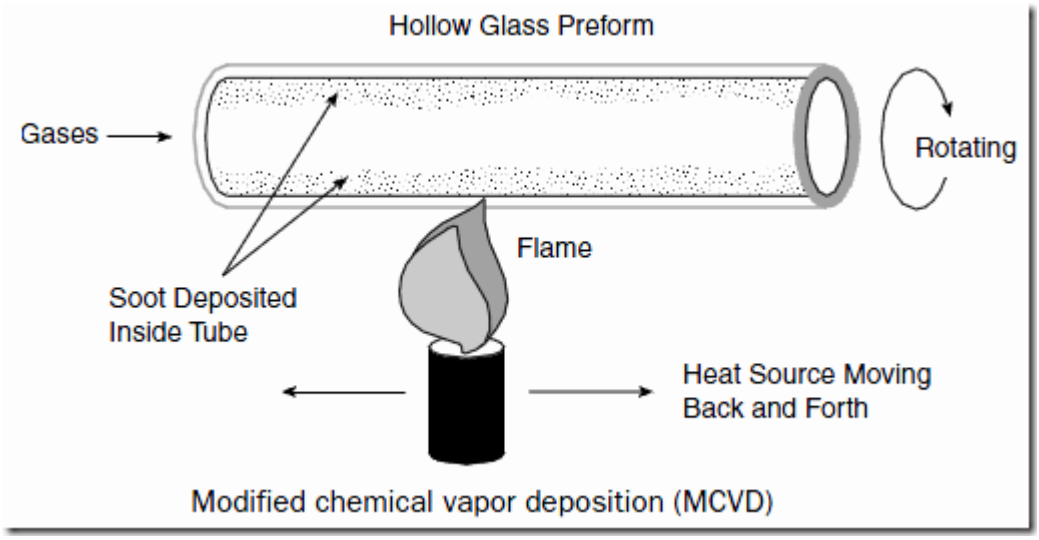

Figure 3.6 [20]: This picture shows the main process of the MCVD technique.

4 Basic theory on the measuring techniques and experimental arrangement

4.1 Basic theory

4.1.1Temperature effect

From the Jablonski energy diagram of figure 2.5, the transitions can be divided into non-radiative and radiation. The radiation transition will emit or absorb photons when the atom transition in different energy levels. But for non-radiative transition, the electrons exchange energy through collisions. There is no photon appears in non-radiative transition. With the temperature increases, the probability of collision will increase. Therefore, the non-radiative transition will increase with temperature. For radiation transition, the temperature effect is quite small.

The decay time is the time electrons stay in the excited state which includes the radiation part and the non-radiative part. The relationship can be described as

$$\Gamma_{tot} = \Gamma_{rad} + \Gamma_{nrad}$$

$$\tau_{total} = \frac{1}{\Gamma_{tot}}$$

where Γ_{tot} is the total decay rate, Γ_{rad} is the radiative decay rate, Γ_{nrad} is the non-radiative decay rate. τ is the measured decay time of the fluorescence.

When temperature increases, the non-radiative transition increases and the radiative

transition do not change. Hence the decay time will decrease with temperature increase.

The transitions probability which is related to the decay time is also related to the temperature change.

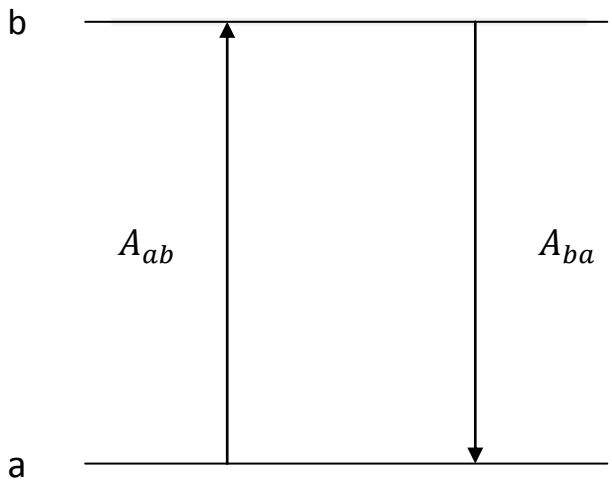

Figure 4.1: This diagram illustrates the emission and absorption transition probabilities between level a and b with the spontaneous transitions probability A_{ba}.

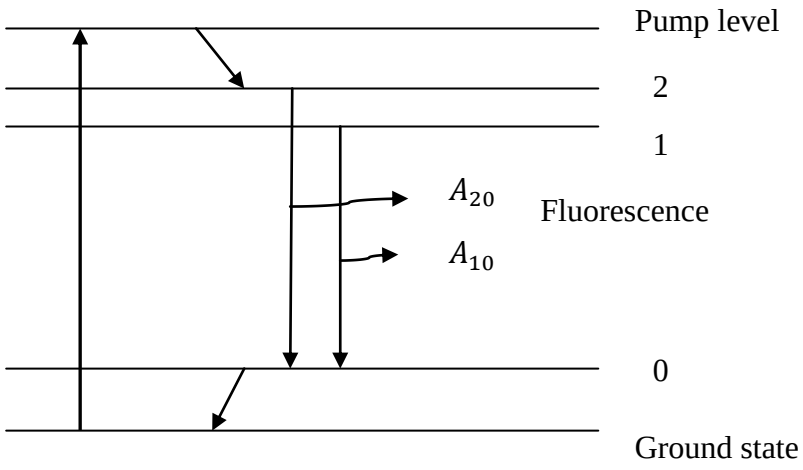

Figure 4.2 : This energy level shows the three level model and the relevant transitions.

The relationship between the decay time and the spontaneous radiation probability is

$$\tau = \frac{1}{A}$$

where τ is the decay time and A is the spontaneous radiation constant (spontaneous radiation probability). Using the relationship between τ and A,

$$n_2 A_{20} \tau_{20} + n_1 A_{10} \tau_{10} = n_2 + n_1$$

where n_1 is the population of level 1, n_2 is the population of level 2.

The ratio of the population of these two levels could be written as

$$\frac{n_2}{n_1} = \frac{g_2}{g_1} exp\left(-\frac{\Delta E}{kT}\right)$$

where g_1 is the degeneracy of level 1, g_2 is the degeneracy of level 2. ΔE is the energy gap between level 1 and 2 and T is the absolute temperature.

When at thermal equilibrium, level 1 and 2 have the same decay time. The new equation is

$$\tau = \frac{1+\frac{g_2}{g_1} exp\left(-\frac{\Delta E}{kT}\right)}{A_{10}+A_{20}\frac{g_2}{g_1} exp\left(-\frac{\Delta E}{kT}\right)} \quad (4.1)$$

The coefficient A is related to the wave function of the energy level and the wave function is sensitive to the local environment. Hence the coefficient A is affected by temperature.

4.1.2 Stress effect

When the fibre is subjected to stress, the shape of the lattice is affected. The local environment change causes changes to the wave function of energy levels, so the coefficient A (spontaneous transitions probability) is affected by stress. From the equation 4.1, the decay time is affected by stress.

4.2 Experiment arrangements

4.2.1 Introduction

This part introduces the devices used in the experiments and the arrangement of the experiments.

4.2.2 Experiments details

This chapter shows the experimental arrangements used to measure the fluorescence of Pr^{3+} doped optical fibre in different temperatures and stress. Either an OPO laser or an Argon-ion laser is used in this project as the excitation source.

An Optical parametric oscillator (OPO) laser is used to excite the Pr^{3+} doped optical fibre at around 480 nm. OPO laser has two separate tunable frequencies light output. The light which has higher energy is called the signal, and the other output is the idler. The combined frequency range is from 400 nm to 2000nm. The signal output is used in this experiment. The OPO laser is pumped by the 3^{rd} harmonic

output of a Nd:YAG laser (Continuum SLIII-10). The max output power is 45 mJ at 445 nm and 12mJ at 780nm. Pulse duration is 10 ns and pulse repetition rate is 10 Hz.

For the OPO laser, pulse to pulse intensity varies a lot. Hence averaging technique is necessary to reduce the fluorescence intensity fluctuation. This can be overcome in parts by using the continuous-wave-Argon-ion laser. However, it has much lower output power.

The 488 nm output of an Argon-ion laser (Coherent Innova 70) is used in the experiments, and it has a maximum output of about 300mW. A mechanical chopper is used to produce pulse excitation for decay time measurements.

The spectrometer (0.125m) cannot isolate cleanly the weak fluorescence from the strong scattering of the laser hence an optical filter OG550 is placed in front of the spectrometer to block out the laser wavelength.

In the emission measurements, the fibre is excited at a particular wavelength and the spectrometer is scanned to record the emission wavelengths. Whereas, in excitation measurements, the fluorescence is monitored at a particular wavelength and the laser wavelength is scanned producing a spectrum similar to an absorption spectrum.

In the decay time measurement, a digital oscilloscope (300 MHz LeCroy 9310) is used to records the data and transfer to the computer for storage and analysis. All the measurements are averaged over 1000 times (at 10 Hz reception rate it takes 100 sec for each decay time measurement). Two decay times were identified in the decay time measurements. The slow decay time is measured using a 5000 Ω terminating resistor, whereas the fast decay time is measured with a 10000 Ω terminating

resistor. Figure 4.3 shows the system respond as a function of terminating resistors. Higher terminating resistor has longer respond time, but it could produce larger signal. The signal of the fast decay time is very weak hence higher terminating resistor was chosen in the experiments. This is a compromise between the system responds speed and usable signal.

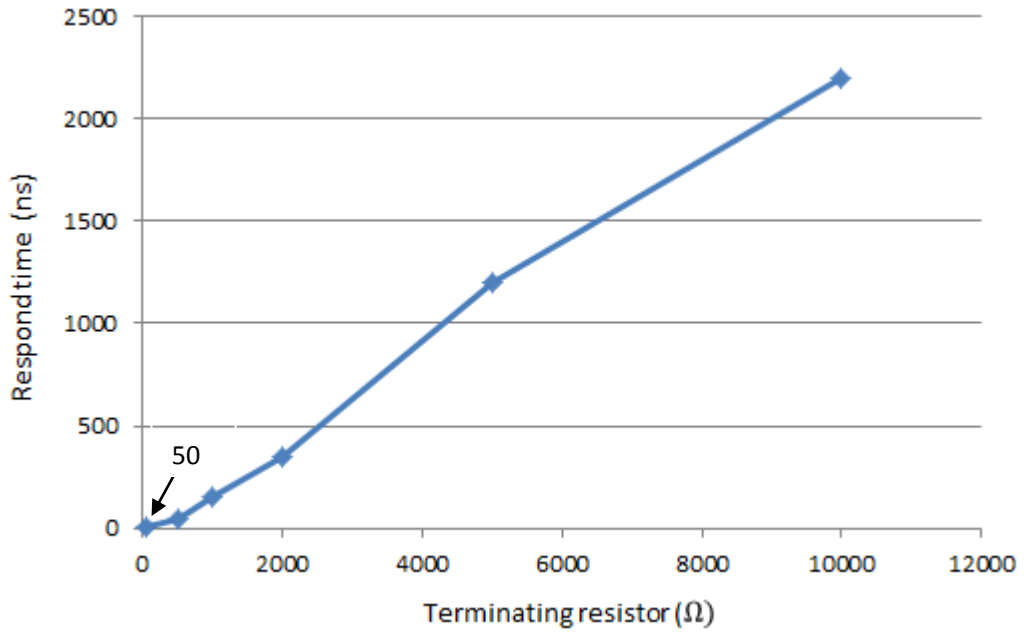

Figure 4.3: This diagram shows the system respond time as a function of terminating resistors (the mark in the diagram means the value of the first data point is 50).

4.2.3 Temperature measurement

In order to heat the fibre evenly, the fibre is submerged in a water bath. A reasonable temperature range from 1℃~90 ℃ can be achieved using a combination of an electric hot plate heater and addition of ice cubes.

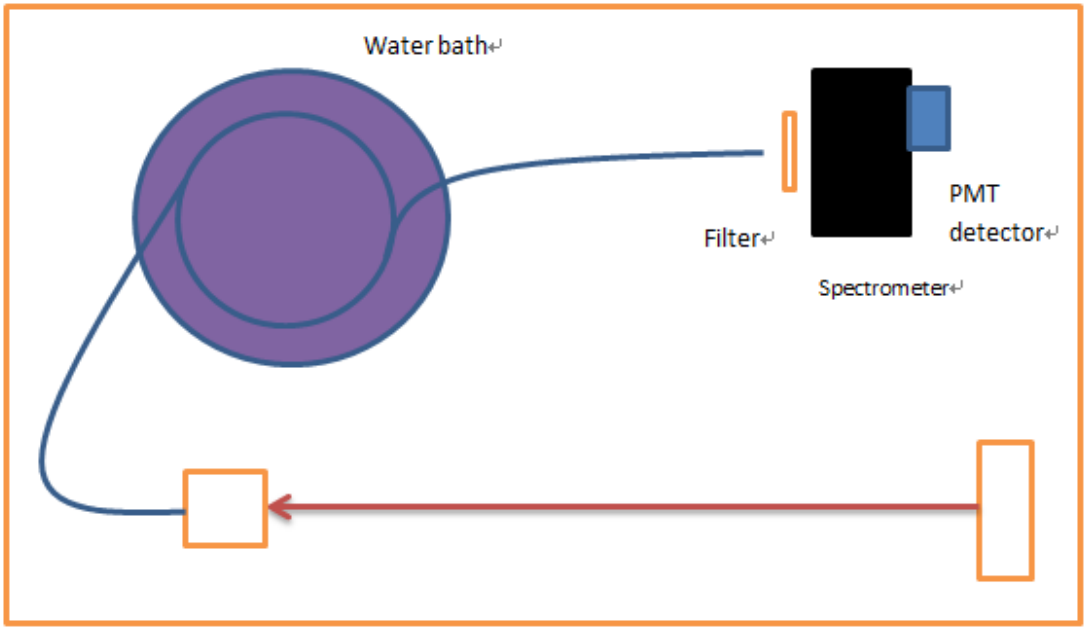

Figure 4.4: Schematic diagram showing the experimental setup of temperature measurement.

4.2.4 Stress measurement

In the stress part, it could be divided into two parts. One is to stretch the fibre and the other is to compress the fibre. For these preliminary measurements the goal is to determine whether there is any observable change and how large are the changes with respect to stretch or compression being applied. To stretch the fibre, a pulley block system isused as shown in Figure 4.5. The fibre is arranged on the pulley, and the weight is put on the moveable block. The weight range is 0-900g.

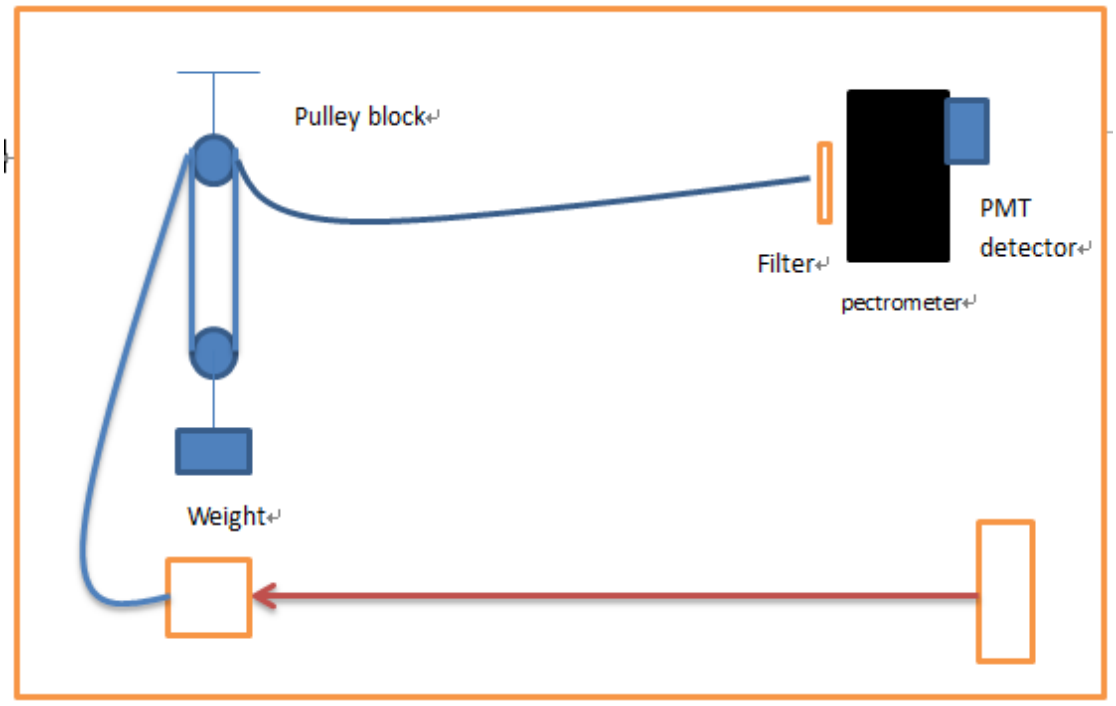

Figure 4.5: Schematic diagram showing the experimental setup of stretch measurement.

To compress the fibre, the fibre is pressed between two wooden blocks with smooth formica surface and the length is same to the stretch method. The force direction is opposed to the stretch method. Figure 4.6 shows the experiment arrangement and how the fibre put in the board. The weight ranges up to 45 kg (a test fibre was used to make sure the fibre will not be crushed at this weight).

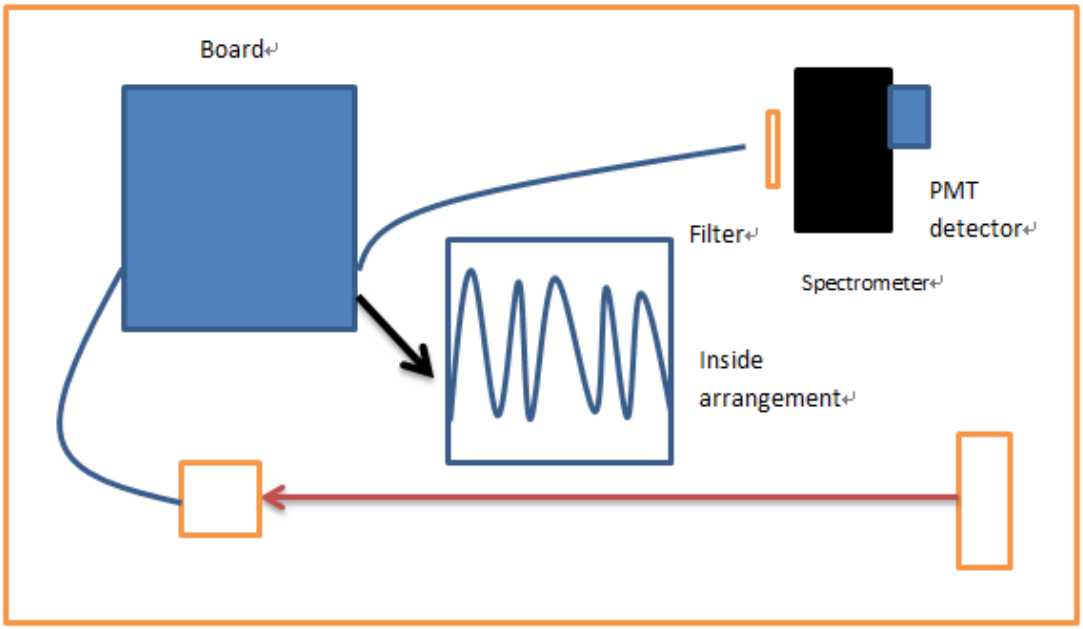

Figure 4.6: Schematic diagram showing the experimental setup of compression measurement.

5 Experimental results

5.1 Introduction

An emission spectrum excited by the 483 nm laser light shows three emission peaks, these peaks are assigned based on Percival's work, see figure 5.1. Compared to Percival's work, the wavelength of peak C is shorter [21]. The reason could be the accuray of the spectrameter is low when the wavelength is higher than 800 nm.

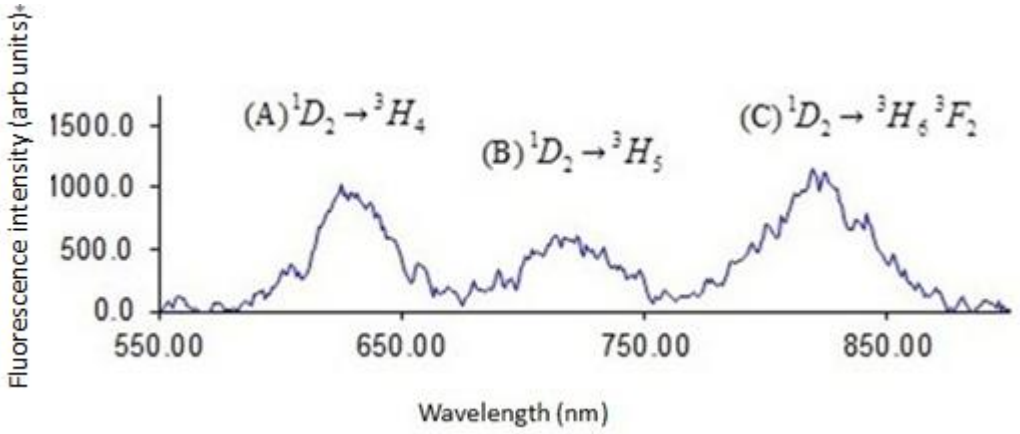

Figure 5.1: This diagram shows the emission spectrum of the Pr^{3+} doped optical fibre. Peak A is the transition $^1D_2 \rightarrow {}^3H_4$, peak B is the transition $^1D_2 \rightarrow {}^3H_5$, peak C is the transitions $^1D_2 \rightarrow {}^3H_6\,{}^3F_2$.

In figure 5.1, peak A shows the transition $^1D_2 \rightarrow {}^3H_4$, but at this wavelength it may also occur transition $^3\mathrm{P}_0 \rightarrow {}^3\mathrm{H}_6\,{}^3\mathrm{F}_2$. Due to $^3\mathrm{P}_0$ energy level fluoresce is very weak in silica hosts, so this transition is not considered in the experiments.

Figure 5.2 shows the excitation spectrum with the spectrometer monitoring at 625nm (peak A). Peak D wavelength is about 473 nm. The excitation spectra for the three

peaks, A, B and C, are very similar and only show slight differences in the intensity.

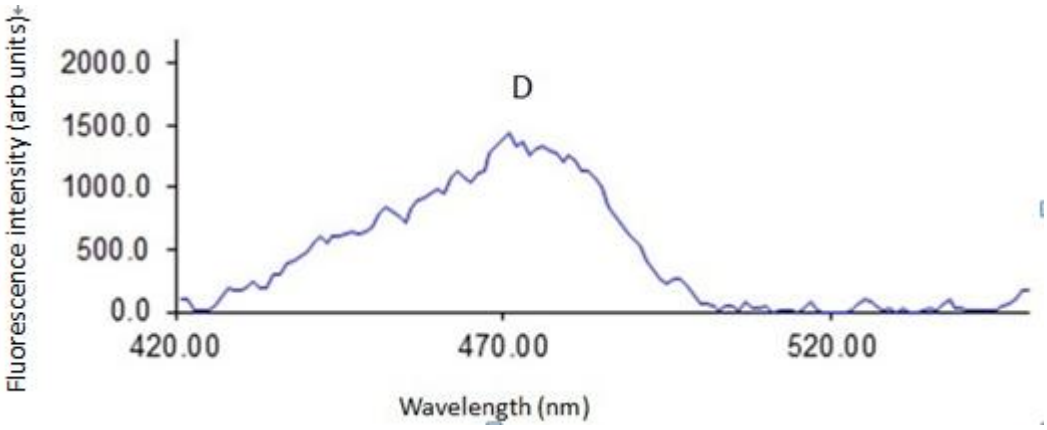

Figure 5.2: Excitation spectrum of the Pr^{3+} doped optical fibre for emission at 625nm.

5.2 Frequency measurements

5.2.1 Temperature results (OPO laser)

The fibre is excited at 472 nm using the OPO laser. Emission peaks A and B are measured at 2℃, 19℃, 33℃, 45℃, 60℃, 76℃ and 98℃. Peak C is measured at 19℃, 33℃, 45℃, 60℃, 76℃ and 98℃. Both of the excitation and the emission spectra are recorded in this part.

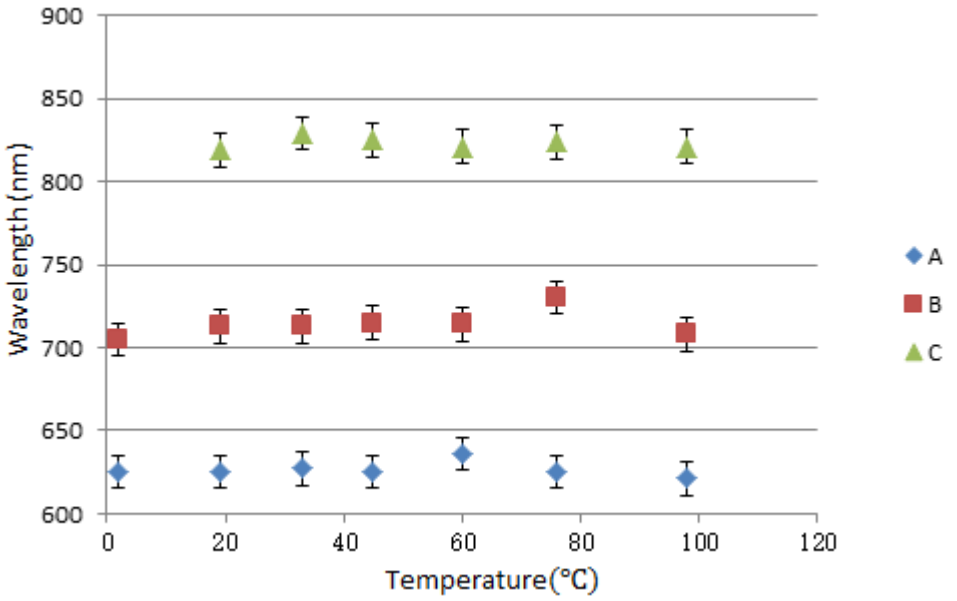

Figure 5.3: The peak position of the emission peak A, B and C as a function of temperature.

It is clear from figure 5.3 that the peak position of the emission lines A, B and C does not change, within the uncertainties of the measurements, with temperatures.

The excitation spectrum is obtained when monitoring the emission at 625nm. Figure 5.4 shows the peak wavelength position of the excitation peak, D, at different temperature.

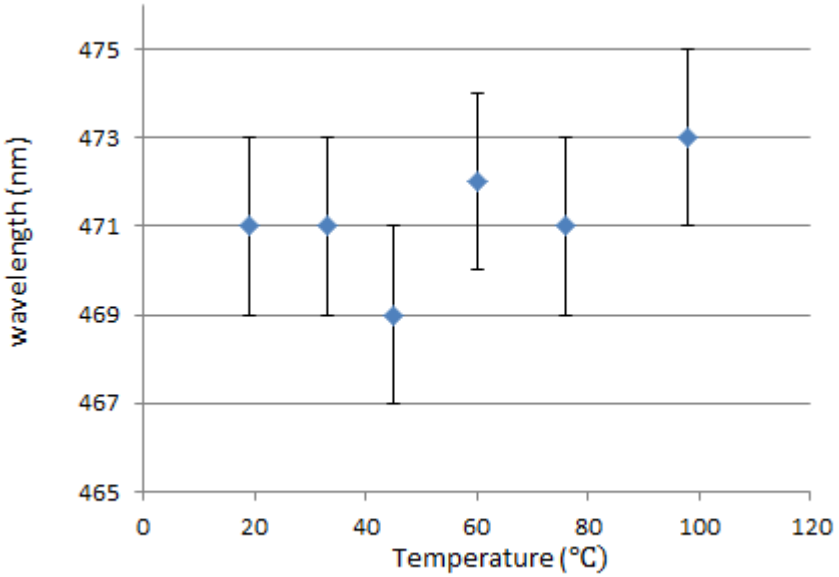

Figure 5.4: The peak positions of the excitation, peak D, as a function of temperature.

Similar to the emission spectra, the changes in the wavelength of the excitation peak with temperature do not follow any pattern and can be consider as no change within the uncertainty of the measurements. The large uncertainties are due to the intensity of the OPO laser output is not stable and even with a smoothing time constant of 3s the noise level is still quite large.

5.2.2 Temperature measurements (Argon laser)

Due to the emission spectra excited using the Argon-ion laser have less noise effect; the line width, full width at half maximum (FWHM) of three emission peaks could be measured.

The fibre is excited at 488 nm using the cw Argon-ion laser. The emission spectra are measured at 19℃, 33℃, 50℃, 68℃, 82℃, 94℃. Figure 5.5 shows the wavelength of the three emission peaks, A, B and C, as a function of temperature. This confirmed

the observation using the OPO laser, figure 5.3, that no observable change or pattern of change, within experimental uncertainties, can be seen.

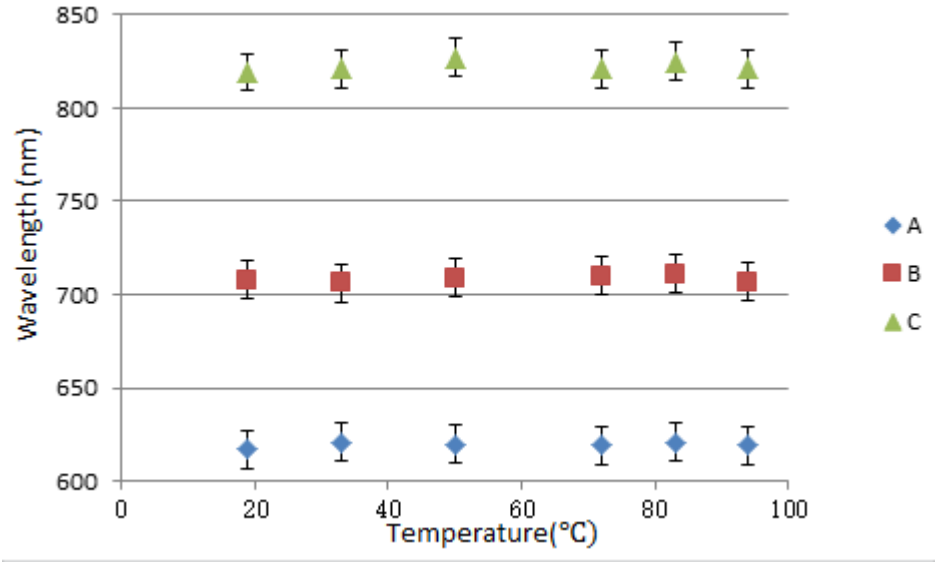

Figure 5.5: The peak positions of the emission peak A, B and C as a function of temperature using Argon ion laser.

Figure 5.6 shows the FWHM of the three emission peaks as a function of temperature.

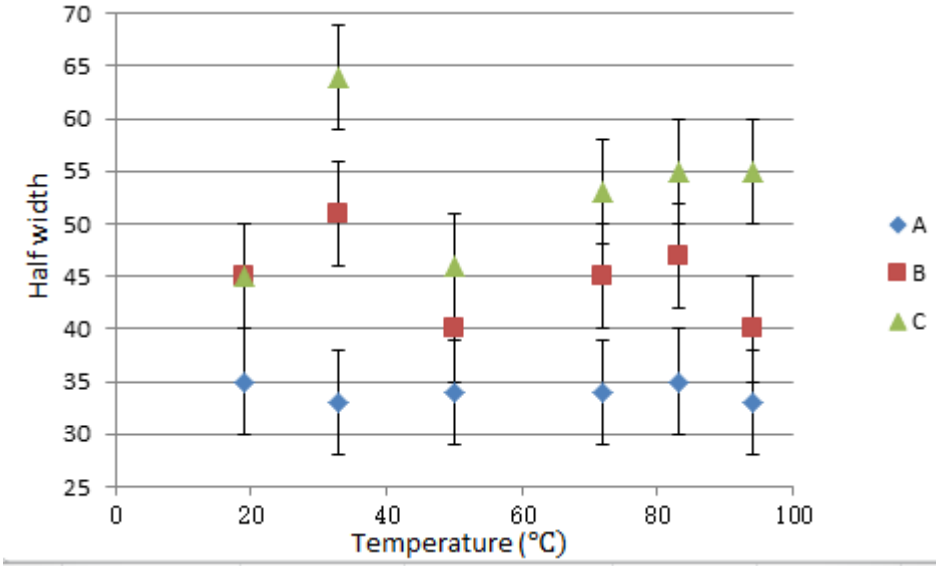

Figure 5.6: The FWHM of three emission peaks at different temperature.

The variation of the FWHM of peaks A and B are within the uncertainties of the measurements. The FWHM of peak C shows observable change, but the variation does not follow any pattern. Compare to peak A, the intensity of peak B and C is quite low. The FWHM measurements of peak B and C is not very precise because of their low signal to noise ratio.

5.2.3 Stress measurement (OPO laser)

The fibre is excited by the OPO laser at 483 nm. The emission spectra for the stretch method were measured for weights ranged from 0 to 900 g in steps of 100g. Figure 5.7 shows the emission wavelength change of the three emission peaks with applied weight. The wavelength of the three emission peaks has no observable changes, within experiments uncertainties.

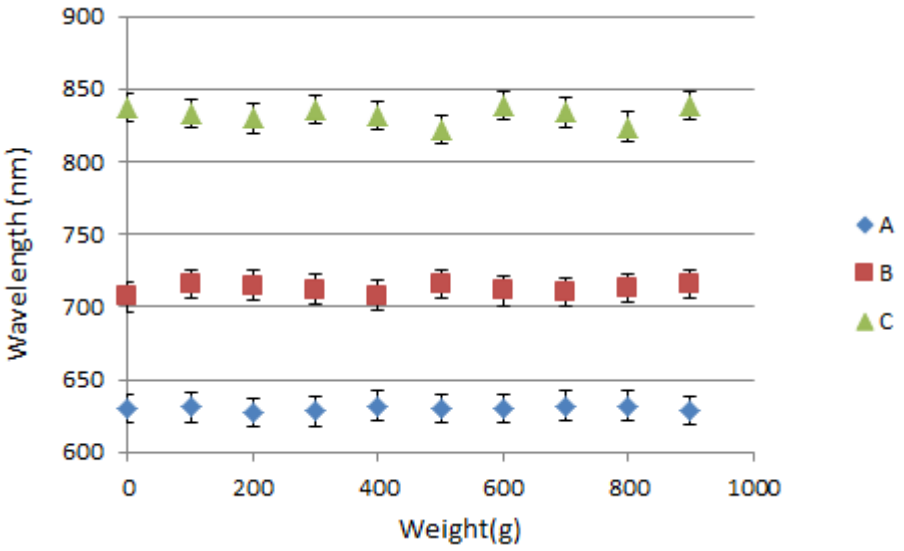

Figure 5.7: This diagram shows the wavelength of the three peaks with different weight.

Figure 5.8 shows the excitation specrum with the detection wavelength at 628 nm.

The wavelength of the excition peak also show no observiable change within the uncertainty of the measurements.

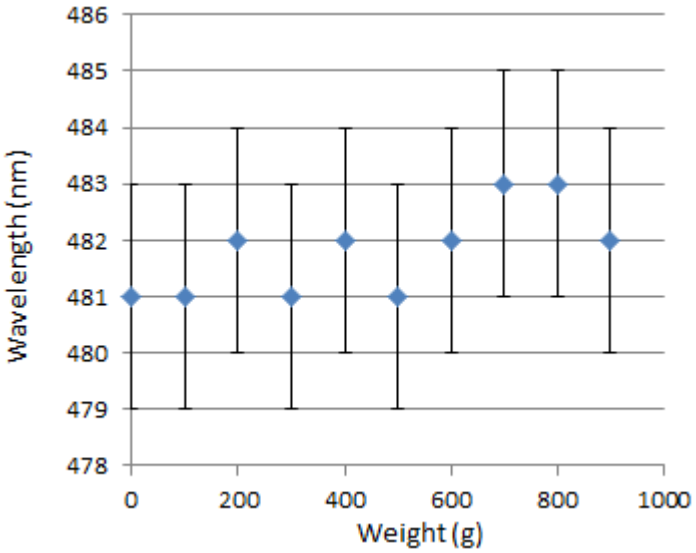

Figure 5.8: This diagram shows the wavelength change of the excition peak with different weight.

5.2.4 Stress measurement (Argon laser)

The weight change is from 50 to 450 g in steps of 100 g. There is no obvirous change shown in figure 5.7, so the measure range is only used to detect if there is any change. The fibre is excited by the Argon laser at 488 nm. Figure 5.9 shows the three emission wavelength of three peaks under different weight. Even though the experimental uncertainties have much reduced when compare to those using the OPO laser, there is still no observable change in the variation of the wavelength of the three emission peaks.

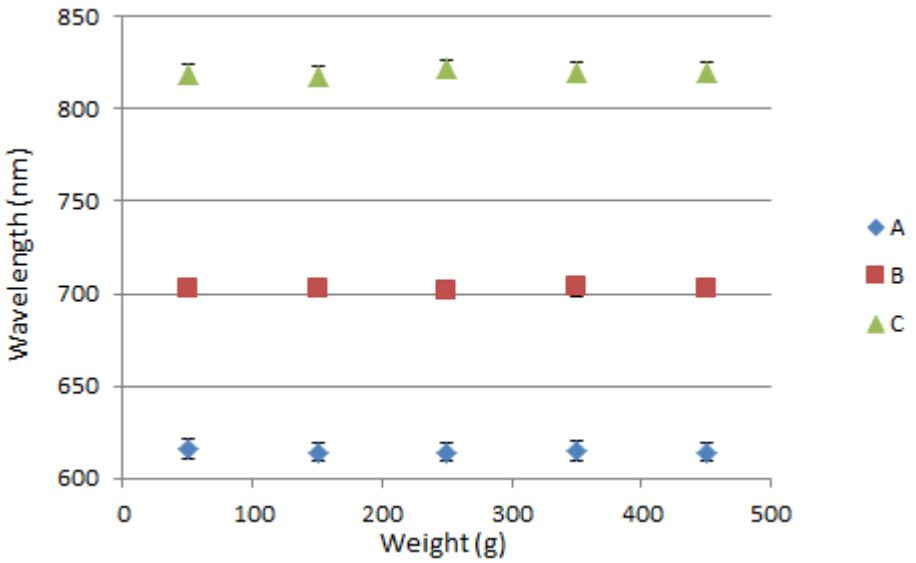

Figure 5.9: This diagram shows the three peaks wavelength change in the emission spectra with weight.

5.3 Decay time measurement

5.3.1 Temperature measurement

The temperature measurements are measured at 20℃, 48℃, 82℃ and 99℃ using the OPO laser at 483 nm as the excitation source. Every decay time result is an average of six measurements (each measurement is an average of 1000 shots). The decay times for peak A (630nm) and C (830nm) were measured. Due to the low intensity of peak B, its decay time was not measured. Figure 5.10 shows the average value of the fast component of the decay time as a function of temperature.

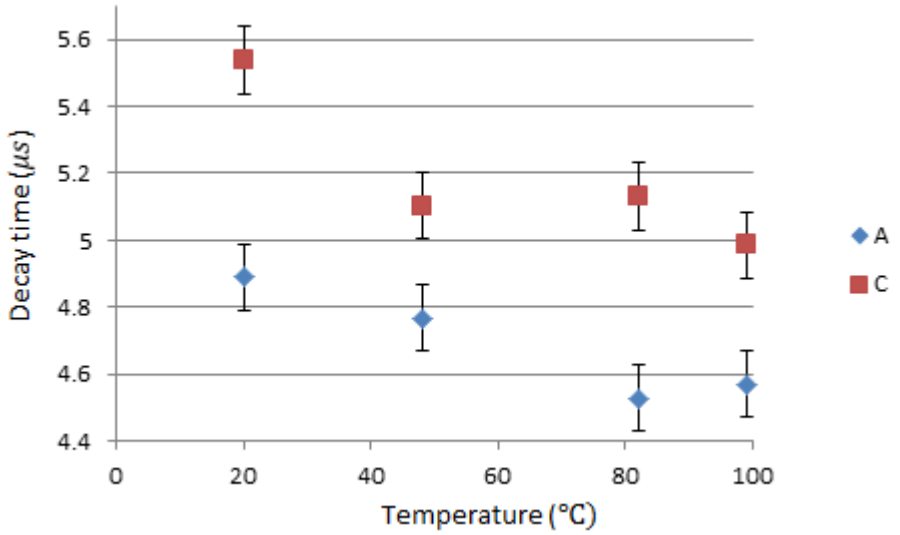

Figure 5.10: This diagram shows the average value of fast component of the decay time as a function of temperature.

The fast component of the decay time for peak A and C both decrease with temperature increase. The decay time of peak C is slightly longer than the one of peak A. For peak C, the fast component of the decay time changes 0.6μs over 80℃ which is very small. Similarly, the fast component of the decay time of peak A change is also very small.

Figure 5.11 shows, the slow component of the decay time of peak A decreases from 20 to 48℃, then keep increasing from 48 to 99℃. For peak C, the decay time increases from 20 to 82℃, then it decreases from 82 to 99℃. Both the slow component of the decay time of peak A and C show large changes, but no pattern can be observed. At present it is unclear the reason for these clearly detectable variation and more work is needed to understand and to resolve this matter. The temperature measure range could be larger and longer fibre could be used in the future research.

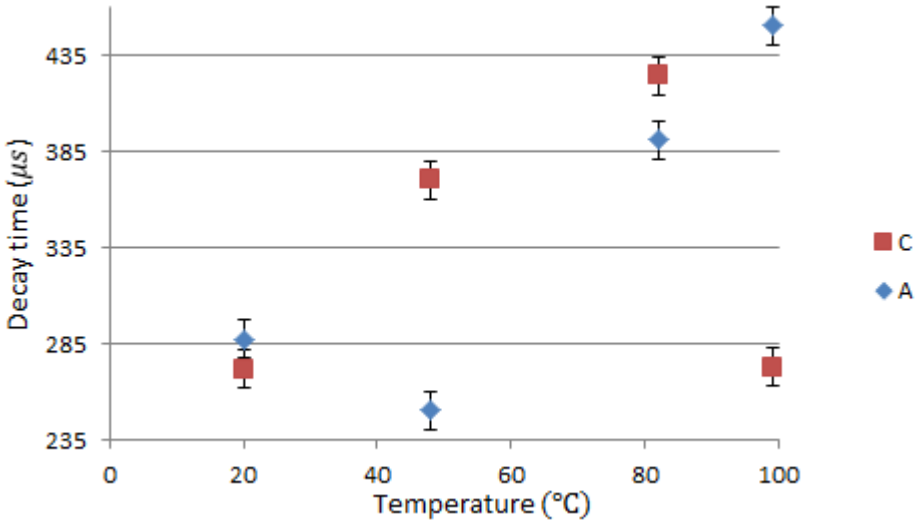

Figure 5.11: This diagram shows the average value of slow component of the decay time.

5.3.2 Stress measurement

The stress measurements are divided into two parts: the stretch and the compression. Both of them are measured at room temperature. Due to the fibre could not hold too much weight with the stretch method, the compression method is used to measure high weight range. For both of methods, the fibre is excited at 483 nm with OPO laser. Emission peaks A and C are both measured in this part.

5.3.2.1 Stretch method

Figure 5.12 shows the fast component of the decay time measured of peaks A and C. The decay time is measured with applied weight from 0 to 900g in steps of 100g.

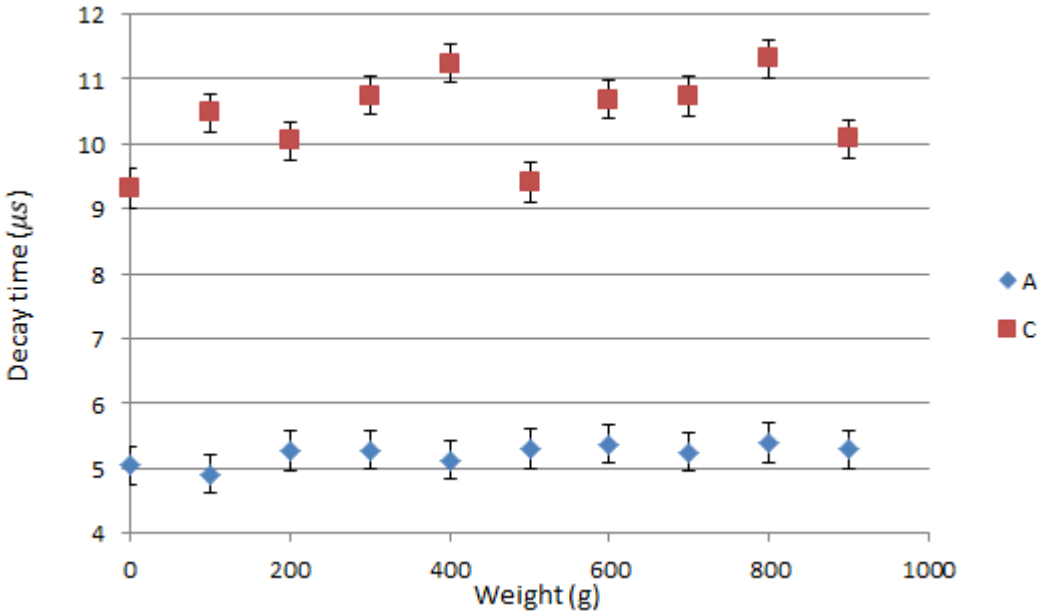

Figure 5.12: This diagram shows the fast component of the decay time of peak A and C as a function of stretch.

For peak A, there is a very slight observable increase in decay time over the full weight range, but the change is very small. This means poor sensitivity and resolution. For peak C, the fast component of the decay time shows an observable change, but the change does not follow any pattern.

The signal of peak C is quite weak, the signal of the fast component of decay time is even weaker. The fast component of decay time of peak C changes very much in each measurements. The fast component of decay time of peak A is more stable compared to peak C.

Figure 5.13 shows the slow component of the decay time measured of the emission peaks A and C. The decay times are measured with applied weight from 0 to 450g.

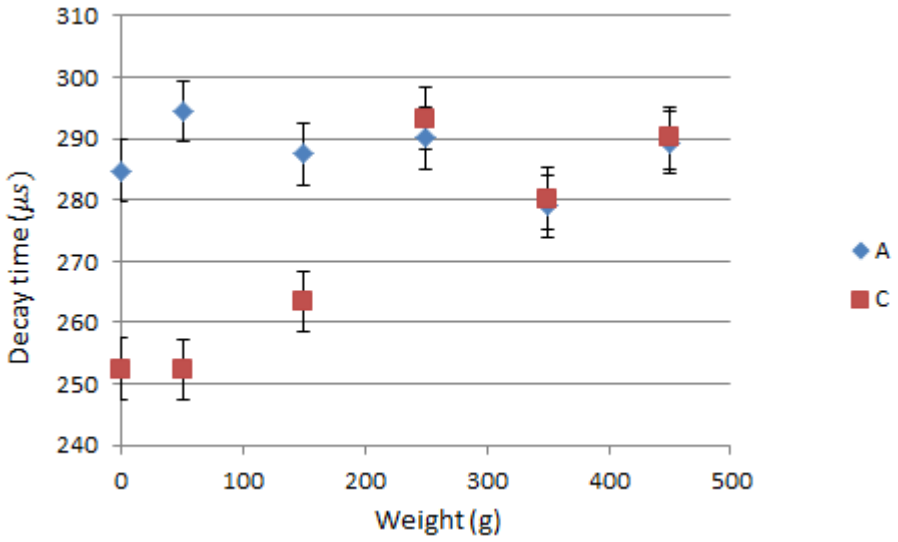

Figure 5.13: This diagram shows the slow component of the decay time of peak A and C as a function of stretch.

The slow component of the decay time of peak A does not show any changes, within the uncertainties, over the applied range of weight. For emission peak C, the slow component of the decay time shows clearly observable change over the applied weight range, about 38μs over 450g.

5.3.2.2 Compression method

The compression method is used to measure the decay time change for the high weight range. From the stretch measurements, the fast component of the decay time is not expected to change hence only the slow component of the decay time is measured for the compression method.

Figure 5.14 shows the slow component of the decay time of the emission peaks A and C. The decay time are measured with applied weight of 0kg, 1kg, 3kg and 5kg.

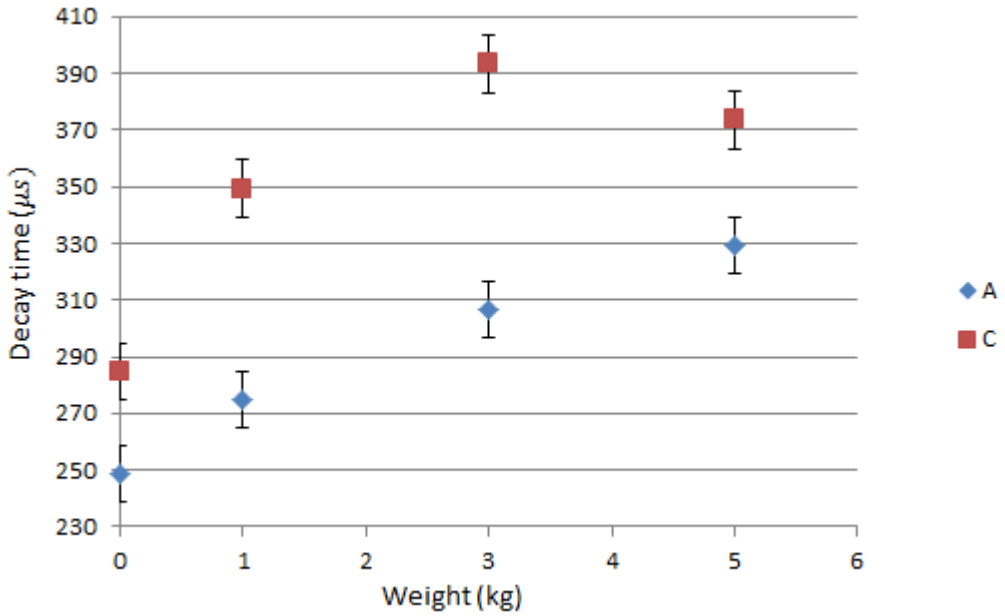

Figure 5.14: This diagram shows the slow component of the decay time of peak A and C.

Both the slow component of the decay time of peaks A and C show a positive trend with increasing weight. For peak A, the decay time changes about 80μs from 0 to 5kg. Compare this to the light weight range, figure 5.13, where no observable change was observed shows that it is only usable for weight range over 500g. For peak C, the decay time changes about 90 μs over 5kg. Although the linearity over the applied weight range is nonlinear it still gives a good usable range.

5.4 Summary and discussion

In the frequency measurements, the Pr^{3+} doped glass fibre is excited by an OPO laser or a cw Argon-ion laser. Their results are similar, the wavelengths of the three emission peaks and the excitation peak do not change within the uncertainties of the measurements with applied changes of temperature or stress. The FWHM of peak C show large changes but it does not follow any pattern.

In the temperature measurement, the fast component of the decay time of peak A and C show quite small change. The slow component of the decay time show large changes, but the changes once again do not follow any pattern.

In the stress measurement, the fast component of the decay time of peak A shows very small change for the stretch method whereas peak C shows large changes, but the changes do not follow any pattern. The slow component of the decay time peak A varies within the uncertainties of measurements. The decay time of peak C shows a positive trend with weights. With the compression method, both of the slow component of the decay time of peak A and C show positive trend with weights.

Compared to other rare earth doped optical fibre such as Yb^{3+}, Nd^{3+} and Er^{3+}, the decay time measurements results of Pr^{3+} doped optical fibre show the same trend, the decay time decrease with temperature increasing and increase with stress increasing [1]. In Koziol's work [1], the temperature dependence is similar to our experiment results, but the stress dependency is contrary to our experiment results.

There are some factors that may affect the experiment results. A 10m long Pr^{3+} optical fibre is used in our experiments whereas only a 100mm fibre is used in Koziol's work [1]. The short fibre is used as a point source, but we used a long fibre for the distributed sensor design [22]. The long fibre could be divided into two sections: an effective section which is subject to the change of temperature/stress and an ineffective section which is not subject to the change of temperature/stress. For this project both the effective part and ineffective parts contribute to the fluorescence (frequency and decay time) due to the use of direct single photon excitation and because the experimental setup is to measure the fluorescence from the end of the fibre. If the length of effective section is much larger than the ineffective section, the influence of temperature and stress will be large. If the length of effective section is

only slightly larger than or comparable to the ineffective section, the changes could be too small to detect. The fibre may be not long enough in our experiments hence the signal from the effective section may be too small to measure. The temperature range could have been extended to -180℃ to just below the softening point of the fibre.

6 Conclusion

6.1 Conclusion

The fluorescence wavelengths of the Pr^{3+} doped glass fibre have been measured in a temperature range 0 to 100 ℃ and a weight range 0 to 900 g. The Pr^{3+} doped optical fibre is excited by an OPO laser and a cw Argon laser. The wavelength position of the three emission peaks, their respective line width and excitation spectra are measured in the experiments. All the wavelengths measurements do not show any obvious change within the limits of the applied changes of temperature or stress. Although the FWHM of peak C show large changes, but they do not follow any pattern of change.

The decay time of the fluorescence are measured in a temperature range 20 to 100 ℃, a stretch range 0 to 900 g and a compression range 0 to 5 kg. The intensity of peak B is quite weak, so its decay time is not measured. In the measurements of decay time, both peak A and C show two decay components in their decay time. In the temperature measurement, the fast component of the decay time of peak A and C show a negative trend with temperature, but the change is quite small. The slow component of peak A and C both show large changes, but the changes do not follow any pattern. In the stretch measurement, the fast component of the decay time of peak A only vary within the experimental uncertainties. The fast component of the decay time of peak C shows an observable change, but the change does not follow any pattern. The slow component of the decay time of peak A varies within the uncertainties range. For peak C, the slow component of the decay time shows a positive trend with weights. In the compression measurement, the slow component of the decay time of peak A and C both show a positive trend with weights.

6.2 Further research

There are still more experiments needed in further work. In temperature measurements, the slow components of the decay time show large changes which do not follow any pattern. The reason for these large changes is not clear and more work is needed to resolve this problem. In decay time measurements, two components of decay time are detected. The phenomenon does not show in other people's work hence more detail spectroscopic studies are needed to resolve the origin of these 2 components. The fibre arrangement is also an important problem. A longer optical fibre is needed in the future experiments. The measure range of temperature and stress could be larger in further work. The accuracy of the devices should be improved in the further work, narrow uncertainties range could help to find the results better. At last, the Pr^{3+} fluorozirconate fibres could be used in the further work. $^{3}P_{0}$ and $^{1}G_{4}$ energy levels fluoresce very weakly in silica hosts, but fluorozirconate fibres could solve this problem [1]. These works could help the development of the Pr^{3+} doped optical fibre in sensor applications.

Reference

[1] B. G. Koziol. (2004). "Temperature and strain dependence of fluorescence in praseodymium-doped silica optical fibre", Melbourne: Victoria University.

[2] G.L. Zhou, S.L. E and W.Y. Deng. (2007). "Development and application of optical fiber temperature sensor", Optical communication technology.

[3] M.C. Farriesm, M.E. Fermann, R.I. Lamming, S.B. Poole and D.N. Payne, "Distributed temperature sensor using Nd^{3+}-doped optical fiber", Electron. Lett. 22, 418-419 (1986).

[4] S.A. Wade, S.F. Collins and G.W. Baxter. (2003). "Fluorescence intensity ratio technique for optical fibre point temperature sensing", Journal of Applied Physics.

[5] Brain Culshaw and Alan Kersey. (2008). "Fiber-Optic Sensing: A History Perspective", Lightwave Technology. Vol. 26, pp. 9.

[6] "Fluorescence microscopy – a brief explanation", http://www.scienceinyoureyes.com/index.php?id=79 viewed 14/09/2013

[7] G. Cosa, K-S. Focsaneanu, J. R. N. McLean, J. P. McNamee and J.C. Scaiano. (2001). "Photophysical Properties of Fluorescent DNA-dyes Bound to Single- and Double-stranded DNA in Aqieous Buffered Solution", Photochemistry and Photbiology. Vol. 73, pp. 585-599.

[8] Angelo A. Lamola, Morris Joselow and T. Yamane. (1975). "Zinc Protoporphyrin (ZPP): A Simple, Sensitive, Fluoometric Screening Test for Lead Poisioning",

Clinical Chemists. Vol. 21, pp. 93-97.

[9] C. Le Men. (1995). “Fibre characterization and measurements”, Trends in optical fibre metrology and standards, pp. 353-397.

[10] Optical fibre. http://www.mybestnotes.co.in/notes/optical-fiber.php viewed 14/09/2013

[11] “Fiber optics in premises networks”, http://www.thefoa.org/tech/ref/premises/fiber.html viewed 17/09/2013

[12] Meridian technologies. (2008). “Multimode vs. Singlemode – Fiber Fundamentals”, Systems contractor news.

[13] H. Abramczyk. (2005). “Dispersion phenomena in optical fibers”, Berlin: University of Lodz.

[14] Transition metal. http://www.newworldencyclopedia.org/entry/Transition_metal viewed 19/09/2013

[15] B.R. Judd. (1962). “Optical Absorption Intensities of Rare-Earth Ions”, Physical Review Online Archive. Vols. 125, Issue 3. Pp. 750-761.

[16] “Optical Spectroscopy II Chelated Rare Earth Ions”, http://www.phy.davidson.edu/ModernPhysicsLabs/optspect2a2006.html viewed 20/09/2013

[17] G. Meyer. (1999). “The Unlike Didymium Twins: Chemistry of Praseodymium

and Neodymium", Materials Science Forum. Vols. 315-317, pp. 154-162.

[18] A. M. Helmenstine. "Praseodymium Atom", http://chemistry.about.com/od/elementfacts/ig/Atom-Diagrams/Praseodymium-Atom.htm viewed 21/09/2013

[19] P. Lecoy. (2008). "Fiber-Optic Communications", London: ISTE Ltd.

[20] Optical Fiber Manufacturing. http://www.fiberoptics4sale.com/wordpress/the-manufacturing-of-optical-fiber/ viewed 21/09/2013

[21] R. M. Percival, M. W. Phillips, D. C. Hanna and A. C. Tropper. (1989). "Characterization of spontaneous and stimulated emission from praseodymium (Pr^{3+}) ions doped into silica-based monomode optical fibre", Quantum Electronics. Vol. 25, Issue. 10, pp. 2119-2123.

[22] C. J. Dalzell, T. P. J. Han, I. S. Ruddock and D. B. Hollis. (2012). "Two-photon excited fluorescence in rare-earth doped optical fibre for applications in distributed sensing of temperature", IEEE Sensors Journal Vol12, No. 1, pp. 51-54.